Simple and Versatile Detection of Viruses Using Anodized Alumina Membranes.

Pavan Chaturvedi[a,b], Stacy D. Rodriguez[c], Ivan Vlassiouk[d], Immo A. Hansen[c], Sergei N. Smirnov[a]*

[a] - Department of Chemistry and Biochemistry, New Mexico State University, Las Cruces, New Mexico 88003, United States; [b] - Department of Physics, New Mexico State University, Las Cruces, New Mexico 88003, United States; [c] - Department of Biology, New Mexico State University, Las Cruces, New Mexico 88003, United States; [d] - Oak Ridge National Laboratory, Oak Ridge, Tennessee 37831, United States

Table of Contents

1. Methods

Materials. Aluminum foil 99.997% (200 μm thick) was obtained from Alfa Aesar, MS2 and Qβ bacteriophages were purchased from ATCC. Polyclonal MS2 antibody was purchased from Millipore. 3-aminopropyl-trimethoxysilane (APTS), glutaraldehyde, potassium chloride, ethanol, methanol, 2-(N-morpholino)ethanesulfonic acid (MES), and 4-(2-hydroxyethyl)-1-piperazine ethanesulfonic acid (HEPES) were purchased from Sigma-Aldrich (analytical grade for all). Phosphate buffered saline (PBS) (10 mM Phosphate, 2.7 mM KCl, 140 mM NaCl, pH 7.4) was obtained in tablet form from Bioline (Taunton, MA). Deionized (DI) water was used throughout the experiments for solution preparation, as well as, for cleaning purposes.

MS2 Phage / Qβ Phage propagation. ATCC-recommended procedures were used to propagate the bacteriophages. After recovering the freeze-dried phages, the phages were propagated using agar plates with a soft-agar/host overlay. Approximately 0.5 mL of the concentrated phage was added to the soft agar and the soft agar/host mixture was poured on the set agar plates. The plates were given 24 hours at 37 °C to incubate. The soft agar was removed from the plates after the 24 hour incubation period by scraping. Centrifugation at 1000 rpm for 25 minutes resulted in the separation of a phage-containing supernatant and a sediment containing cellular debris and agar. The supernatant was transferred to a new micro centrifuge tube after being filtrated through a 0.22 μm Milipore filter. The samples were then stored at 4 °C until used. The phages were used within 3 days of propagation.

Sensor Preparation. High-purity Al sheets were used to fabricate the porous anodic alumina membranes. Each small piece (5cm × 2cm × 0.2mm) of Al sheet was first (annealed at 300 °C for 2 h) cleaned in acetone, then 1M NaOH, followed by DI water, and then electropolished in a mixed electrolyte solution of perchloric acid and ethanol (1:3 v:v). After washing in copious

amount of DI water and methanol, the Al sheet was anodized in 3 wt% oxalic acid solution typically at 60 V DC voltage at 4 °C with another Al sheet used as anode. The use of the so-called ''two-step'' method allowed for high periodic arrangement of pores in the resulting alumina membrane. [1-4] Following the first anodization for 1h, the resulting anodized aluminum oxide (AAO) membrane was dissolved in a solution of chromic acid and phosphoric acid (1.8 wt% H_2CrO_4 / 6 % v/v H_3PO_4) at 70 °C. This process leaves an imprint of the periodic array of indentations due to well-arranged pores from the first anodization. The second anodization of the remaining Al sheet, at the same conditions for 315 min resulted in almost hexagonally arranged pores of 30 μm length and with 73 ± 14 nm diameter as shown in Figure S2. The value was obtained by analysis using ImageJ. It agrees well with the typically observed correlation of the diameter to anodizing voltage ratio, D/V ~ 1.2 nm/V. Etching in 5% phosphoric acid at room temperature for 50 min partially dissolved the oxide layer at the bottom of the pores and also widened the pores to a diameter of ~ with 97 ± 17 nm.[5] The rate of etching for this concentration at room temperature is ~0.3 nm/min (at 20 °C)[6] and during 50 min the pores are expected to widen by ~30 nm. Anodization of the Al sheet was done on both sides, which left the Al metal layer in between the AAO membranes that provided the necessary support for the membranes for direct mounting in the electrochemical cell while serving as a working electrode. In the alternative approach, the anodization was finished by thinning of alumina barrier layer with stepwise lowering of the current (electroetching; see Figures S2 and S3) following the previously described procedure.[7] In each current controlled step, the anodization voltage gradually declined which lead to a gradual removal of the oxide layer (see Scheme S1) as the thickness of alumina barrier is proportional to the anodization voltage. [8] The current was step-wise reduced by a factor of 2 in increments lasting *ca.* 7 min. The final step was when the voltage reached below 5 V.

Surface modifications. The anodized membrane was washed several times in DI water and dried for 10 minutes at 120 ºC before modification with 2 w/v% APTS (3-aminopropyl-trimethoxysilane) solution in ethanol for 1 h. After washing several times with ethanol to remove the non-covalently bonded silane, the AAO membrane was baked at 120 ºC for 3 h to ensure the covalent bonding between the alumina and the silane molecules. The first step provided a monolayer of amino-silane in the pores. The remaining steps, sketched in Figure S1, were performed in a homemade electrochemical cell made of 1 cm thick Teflon with a 5 mm diameter hole on top of the membrane. In the next step, 60 µL of 5% aqueous solution of glutaraldehyde was used to activate the aminated surface of the AAO pores by overnight treatment followed by drying with N_2 gas. In the final step, MS2-phage polyclonal antibody was immobilized on the AAO pores using 60 µL of a 50 µg/mL solution for 3 h at 4 ºC.
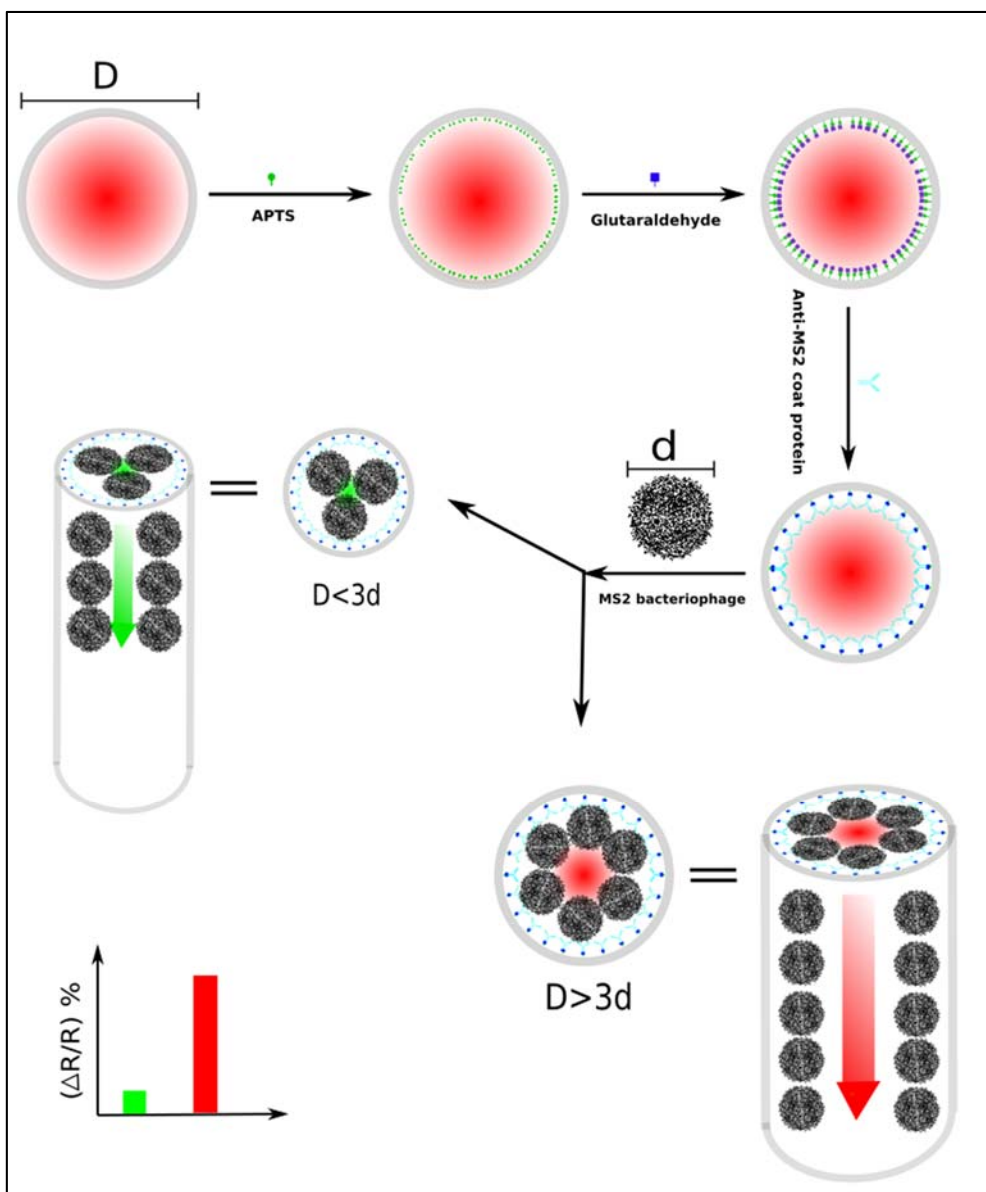
Scheme S1. *Illustration of the sensor preparation and the detection principle.* Pores with diameter D are equipped with the antibody on their walls for a desired virus. The virus particles of diameter d can be captured from a solution but the efficiency of their attachment to the walls and thus pore-blocking is affected by accessibility of the walls to viruses which declines if D < 3d.

2. Pore Etching Treatments and Images of the Pores

Electrochemical etching of the as prepared alumina membranes allows removal of the barrier oxide layer without affecting the pore diameter. It was done using a current controlled scheme was used for that in accordance with literature. The progress was monitored via voltage change and when it stabilized, the current value was dropped by a factor of two. This process was repeated until the lower voltage was obtained as shown in Figure S1. The two possible ways to remove the barrier oxide of the alumina pores were described in Methods lead to different structures as illustrated in Scheme S2.
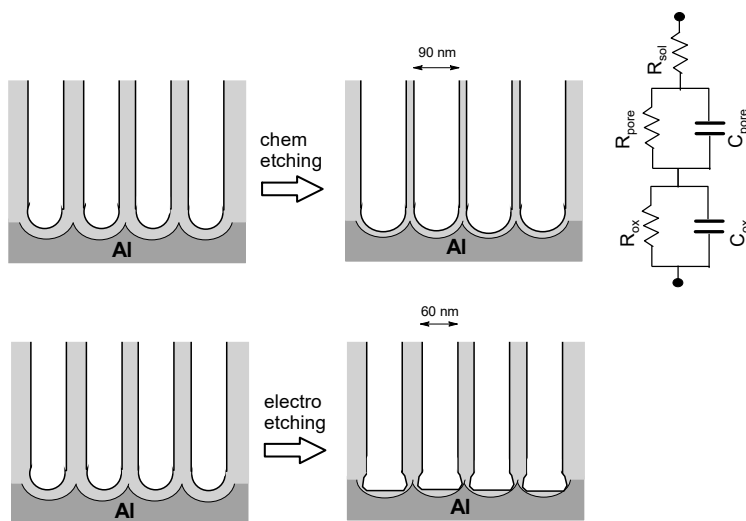
Scheme S2. Illustration of the two types of oxide removal near the Al electrode: chemical etching and electrochemical. The top one (chemical etching) leads to conformal thinning and the corresponding widening of the pores, 97 nm in our case. The bottom one (electro etching) preferentially removes the oxide near the Al electrode and altering the pore diameter, 60 nm in our case. The inset on the right shows the equivalent circuit diagram where R_{sol} is solution resistance above the membrane, R_{pore} and C_{pore} are the resistance and capacitance of the pores in the membrane, and R_{ox} and C_{ox} are the resistance and capacitance of the oxide layer.
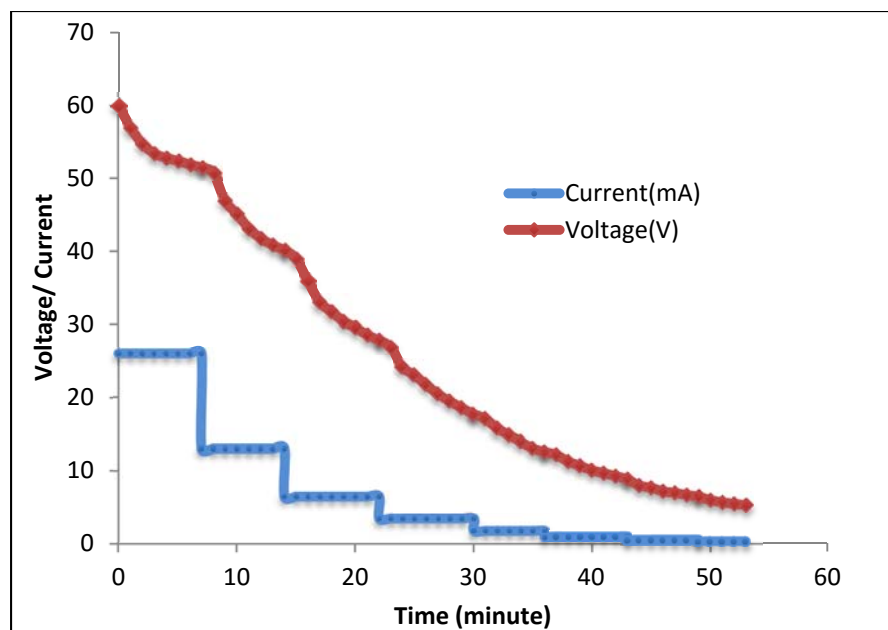
Figure S1. Protocol for electrochemical etching of the oxide barrier layer performed in 0.3 M oxalic acid at room temperature. The controlled current was step wise reduced in a factor of 2 increments lasting *ca*. 7 min.
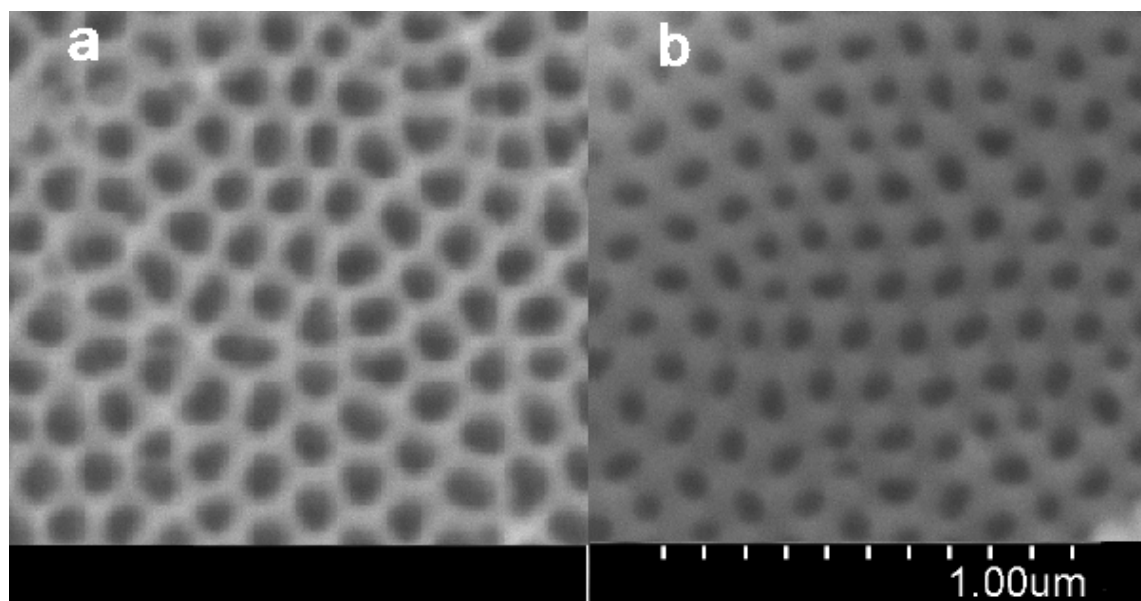

Figure S2. SEM top view of alumina membranes: **a -** chemically etched in phosphoric acid and **b -**electrochemically etched. The pore diameters are 97 ± 17 nm and 73 ± 14 nm, respectively.
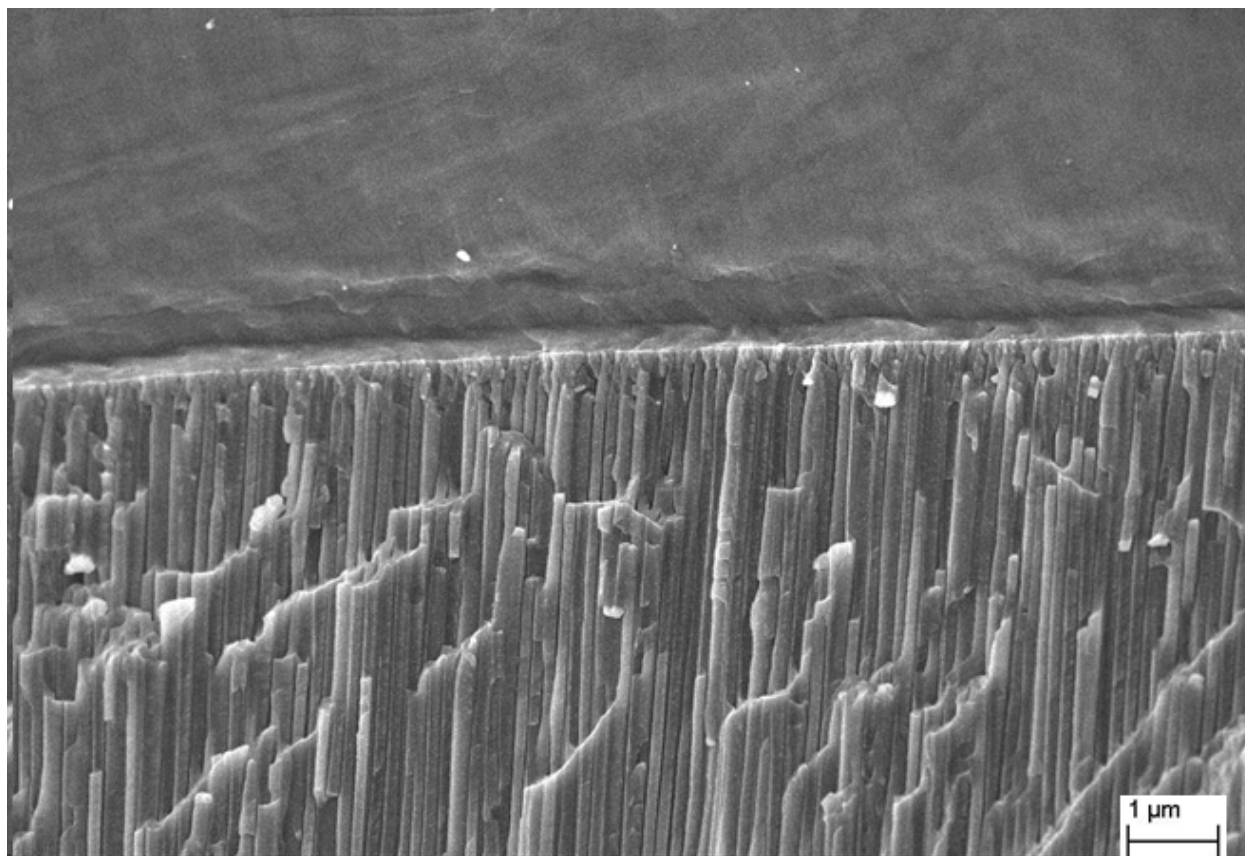
Figure S3. Zoomed in view of the electrochemically etched oxide barrier layer at the end of alumina membrane.
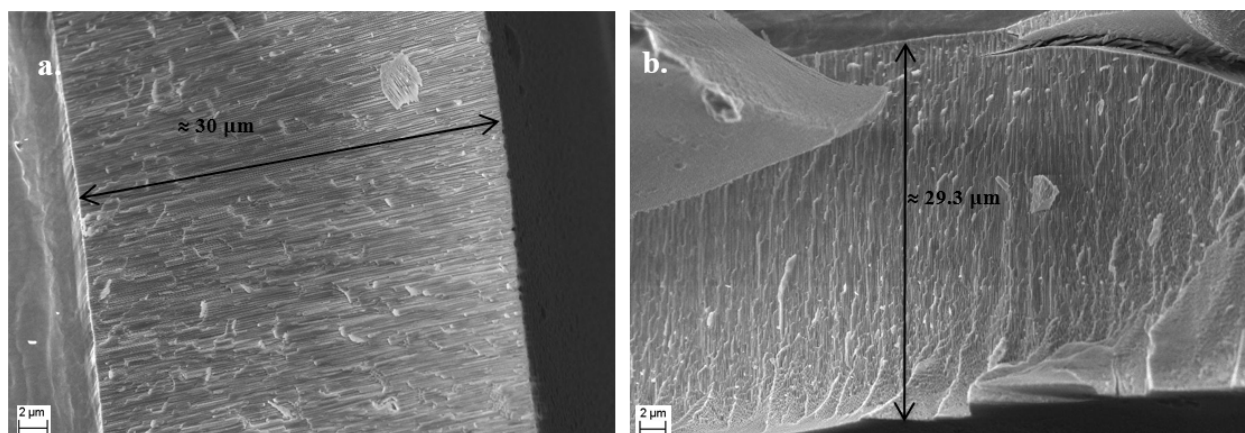

Figure S4. SEM images of the anodized alumina membranes (side view) illustrating their lengths: **a**. after etching in phosphoric acid, **b**. after electrochemical removal of the oxide barrier layer.
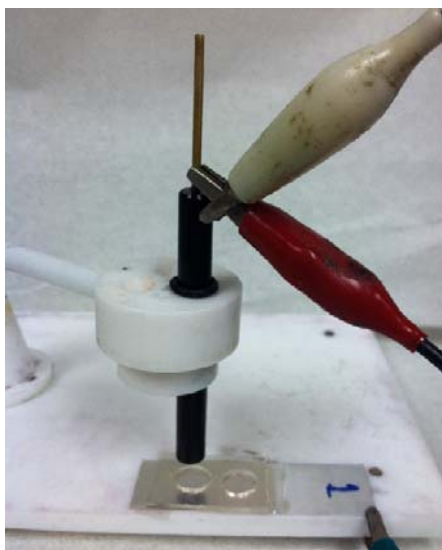
3. Layout of the Cell

Figure S5. A typical layout of the cell used in the experiments. The bottom electrode is prepared from anodized aluminum modified with antibodies, as in Figure S1. The top electrode is either made of a noble metal or identical to the bottom electrode.

4. The Effect of pH on the Sensor Response

In the volume exclusion detection scheme, the surface charge effect (SCE) contribution has to be minimized for the proper detection. The surface charge effect is most strongly present at low electrolyte concentrations when the charge on the pores walls dictates the concentration of counterions inside the pores. The charge on the pores' walls from the ligands and residual incompletely modified groups can be altered by the bound analyte (phages in our case) and affected by pH. Thus high (0.1 M or more) electrolyte concentrations were typically used in our experiments. Nevertheless, even at 0.1M KCl the surface charge due to hydroxyl groups of the AAO membrane and other surface groups introduced during modification, as well as, from captured bacteriophage is not totally minimized in such small pores that are used here. The charge depends on pH and for alumina is close to zero (PZC) at pH ~ 8.5.[9] The pK$_a$ for amines

and Schiff base (resulting from the reaction of amine and glutaraldehyde) are in the similar range. Point of zero charge (pI) for MS2 bacteriophage is between pH 3-4 and the charge of MS2 does not change significantly within the pH range 4-8.[10-12] Thus, in the pH range pH4-pH8 the charges between the species on the surface are: negative on MS2 phage, positive on naked AAO membrane, amines, and Schiff base. The pI of the antibody is unknown.

As seen in Figure S6, measurements in PBS have lower impedances at all stages compared to other buffers, which is due to a greater ionic strength (~ 0.15 M) in comparison to 0.1 M electrolyte for buffers at other pH values. At all pH in the range pH6-8 the impedance drops after amines were activated with glutaraldehyde modifications probably due to a slightly greater pKa of Schiff bases. Further modification with antibody increases the impedance (at all pH in this range) due to a significant volume brought by them but a contribution from the surface charge neutralization can also be a factor depending on pI of the antibody. It might be the reason why the relative increase in the impedance after antibody is the greatest for pH 8, suggesting that pI of the antibody is below 8. After attachment of MS2 phage (60 pfu/mL) the membrane resistance increases in all cases but the relative increase is the highest at pH 6, again, likely due to contribution of charge neutralization with negatively charge MS2. Because not much variation with pH was identified, the majority of measurements were performed in PBS as it is most close to physiological conditions.
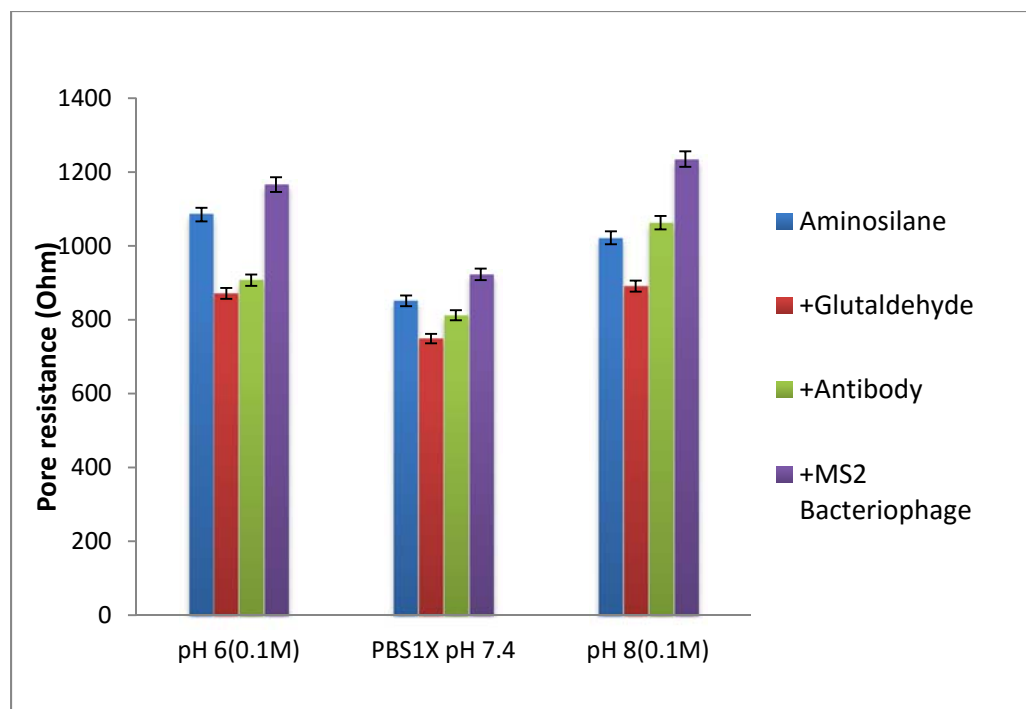
Figure S6. Membrane resistance at 6.2 kHz for different pH at each step of surface modification; 60 pfu/mL of MS2 was used. Electrolyte (KCl) concentrations are shown in the legends.

5. Packing Efficiency in the Pores.

The general problem of the packing efficiency of cylindrical pores by filling them up with spherical particles is different form the one we have here. Since our viral (spherical) particles are attaching to the walls, there has to be a sufficiently large void allowing for the particles to move in and out of the pore. Obviously, the smallest diameter cylindrical pore sufficient for that deed is supposed to be at least three times greater in diameter than the diameter of each sphere:

$$D > 3d \qquad\qquad (S1)$$

Which corresponds to 6 closed packed particles on the perimeter (see Figure S7A). Only in that situation there will be a cylindrical void in the middle with diameter d sufficient for spheres to pass through. The packing fraction (excluded volume) at this point, as illustrated in Figure S8, corresponds to ~ 0.52.

The increase of diameter, D, in general leads to decline in packing efficiency; a particular realization of it can vary. In one scenario, the 6 spheres on the perimeter maintain their C_6 symmetry, which leads to the increase of the gap in between them. The neighboring layers (also in C_6 symmetry) will fill these gaps by coming closer to each other. At first, the packing fraction will decline but eventually start increasing and reach closed packing again for $D \sim 4.34d$ (see Figure S7C). It happens when the neighboring layers on the top and the bottom start touching each other. Alternatively, the spheres can rearrange on that layer to let in an additional one (seventh), which happens when $D \sim 3.30d$. An additional sphere can be added for the following diameters of the cylinder:

$$\frac{D}{d} = 1 + \frac{1}{\sin(\pi/n)} \tag{S2}$$

where n is the number of spheres on the perimeter in one layer. Both scenarios can repeat for $n = 7$ spheres, 8, and so on. In each C_n symmetry case, the second point of closed packing is achieved for:

$$\frac{D}{d} = 1 + \frac{\sqrt{3}}{2\sin(\pi/2n)} \tag{S3}$$

and corresponds to touching of the neighboring layers (see Figure S7C). Figure S8 presents all these solutions for packing fraction, α, as a function of the diameter ratio, D/d, for different n:

$$\alpha = \frac{2n}{3\left(\frac{D}{d}\right)^2 \sqrt{1-\left(\left(\frac{D}{d}-1\right)\sin\left(\frac{\pi}{2n}\right)\right)^2}} \tag{S4}$$

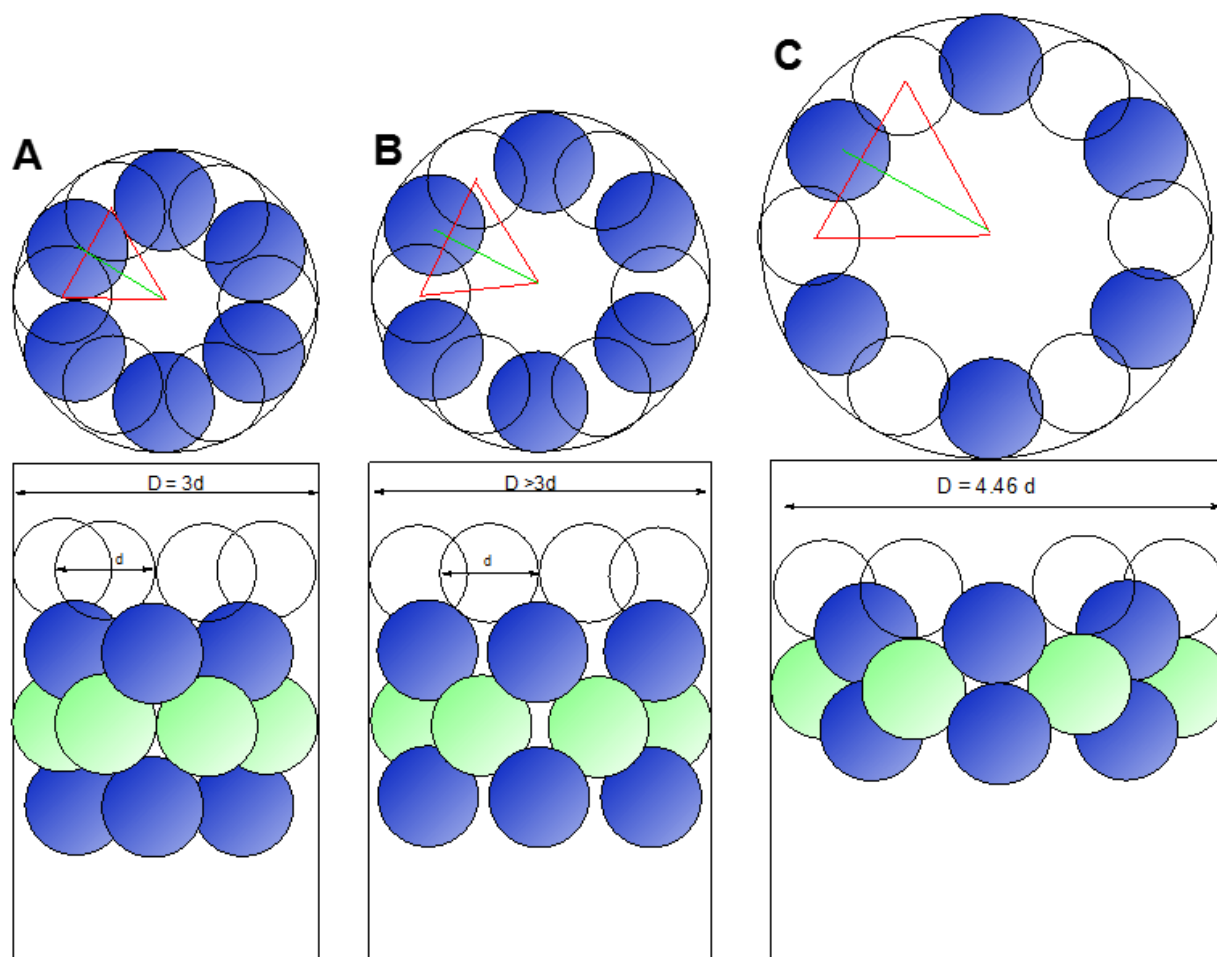The thick line identifies the overall trend with maximum packing fraction.

Figure S7. Illustration of progressive changes in packing of spherical particles on the walls of a cylinder with increasing diameter of the cylinder. It starts with closed packing of 6 viral particles on the perimeter (A). If the C_6 symmetry is maintained, with increasing D, the gap between particles increases with the corresponding decrease in packing (B) but eventually transforms to the closed packed again as illustrated by the blue balls touching each (C).
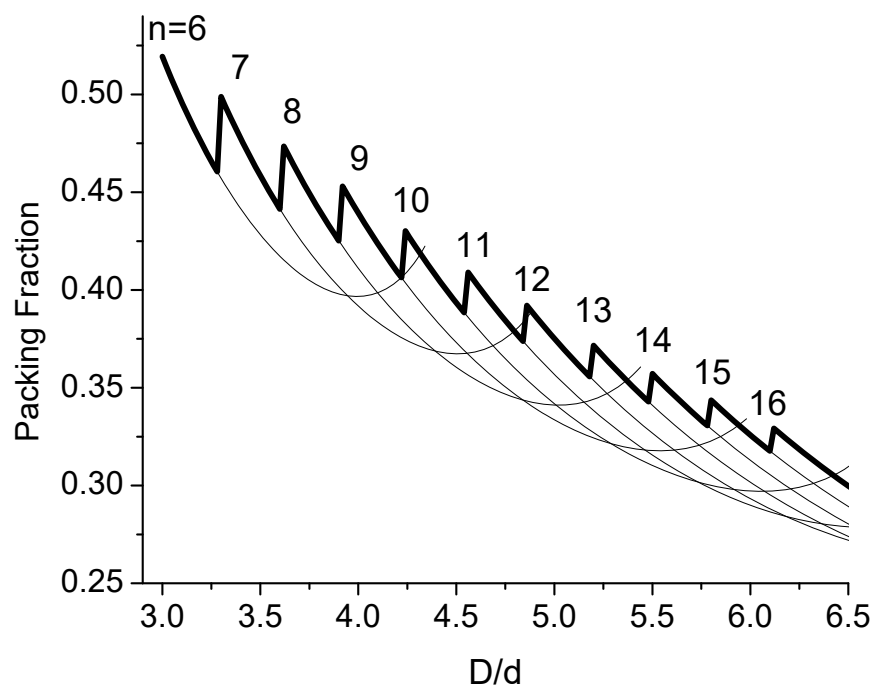
Figure S8. Plot of the packing fraction for the cylinder's volume filled by spherical viral particles attached to the walls as a function of the cylinder's diameter/virus particle. Thin lines represent solutions when C_n symmetry is maintained, where n is identified on the plot. The thick line corresponds to the maximum packing efficiency,

6. Impedance measurements using laptop's sound card

Impedance measurements can be designed using ubiquitous capabilities of a sound card from any laptop and that can be realized using different software. We have explored commercially available software "Daqarta"[13] and "LabView".[14] The former is more specialized for the use of a sound card and thus is easier to implement. All measurements were performed using a laptop with Intel i5 Processor 2.27 GHz, 32-bit operating system, 4GB RAM, running Windows 7

Home edition@2009, with a standard Sound Card, IDT High Definition Audio CODEC and Intel(R) Display Audio.

The sound card allows AC signal generation in the frequency range 20 Hz - 20 kHz with reasonable sampling rate. In the present experiments, the optimal frequency for membrane resistance measurements was 9.6 kHz (or 360 Hz), well within the sound card limits. One can tune the frequency range of the optimal measurements for sensor impedance by varying the pore length and diameter, as well as, by manipulating the oxide removal, as explained in the main text. The resistance value can be further altered/optimized by the overall area of the open section in the membrane and by electrolyte concentration. In our experiments it was in the range R_x = 1-3 kΩ.

The simplest method to perform the measurements is using the voltage divider with a reference resistor, R_o, in series with the measured resistor, R_x. The latter is in parallel with the input resistance of the mic channel, R_L. The driving AC voltage, V_{in}, is supplied from the audio signal output of the sound card and V_{out} is measured through the mic input, as shown in the equivalent scheme below.
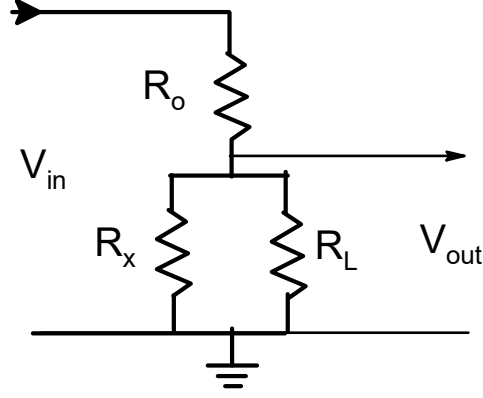
Scheme S3. Equivalent circuit for measuring impedance R_x by utilizing the voltage divider with R_o being the reference resistor. The voltage V_{in} is supplied from the audio signal output of the sound card and V_{out} is measured through the mic input. R_L is its input resistance.

Using the equivalent circuit of Scheme S3, the relative readout signal V_{out}/V_{in} can be related to the three resistances involved via Eq.(S5):

$$\left(\frac{V_{in}}{V_{out}} - 1\right)\left(\frac{1}{R_o}\right) = \frac{1}{R_x} + \frac{1}{R_L} \qquad (S5)$$

The most important imperfections of the setup are the noise and the cross-talk between channels. The noise was particularly sensitive to whether the laptop was plugged in or operated on its battery. The latter configuration was much better, when noise level could be almost neglected. The cross-talk, V_{cross}, between the two channels arose on the sound card itself without any external connections and was practically independent of the driving voltage, V_{in}, magnitude. A smaller magnitude of cross-talk was coming from the external circuit. The overall V_{cross} was never above 2 mV and its contribution for $V_{in} > 0.3$ V could be viewed as almost negligible. Nevertheless, it can be included as given in Eq.(S6):

$$\left(\frac{V_{in}-V_{cross}}{V_{out}-V_{cross}} - 1\right)\left(\frac{1}{R_o}\right) = \frac{1}{R_x} + \frac{1}{R_L} \qquad (S6)$$

Figure S9 shows the plot collected at 6 kHz with V_{in} = 360 mV and R_o = 9.840 kΩ for R$_x$

changing in the range R_x = 1.2-2.5 kΩ. The resulting V$_{out}$ varied in the range V_{out} = 29 - 46 mV

and led to R_L = 3.65 kΩ and V_{cross} = -1.2 mV. The negative sign for V_{cross} indicates that the cross-

talk signal, at least at 6 kHz frequency, has more than 90° phase shift. Since the reference

resistor, R_o, can be cheaply made a part of the sensor, the sound card alone can be conveniently

employed as a measuring device of the proposed impedance sensor. The resistance

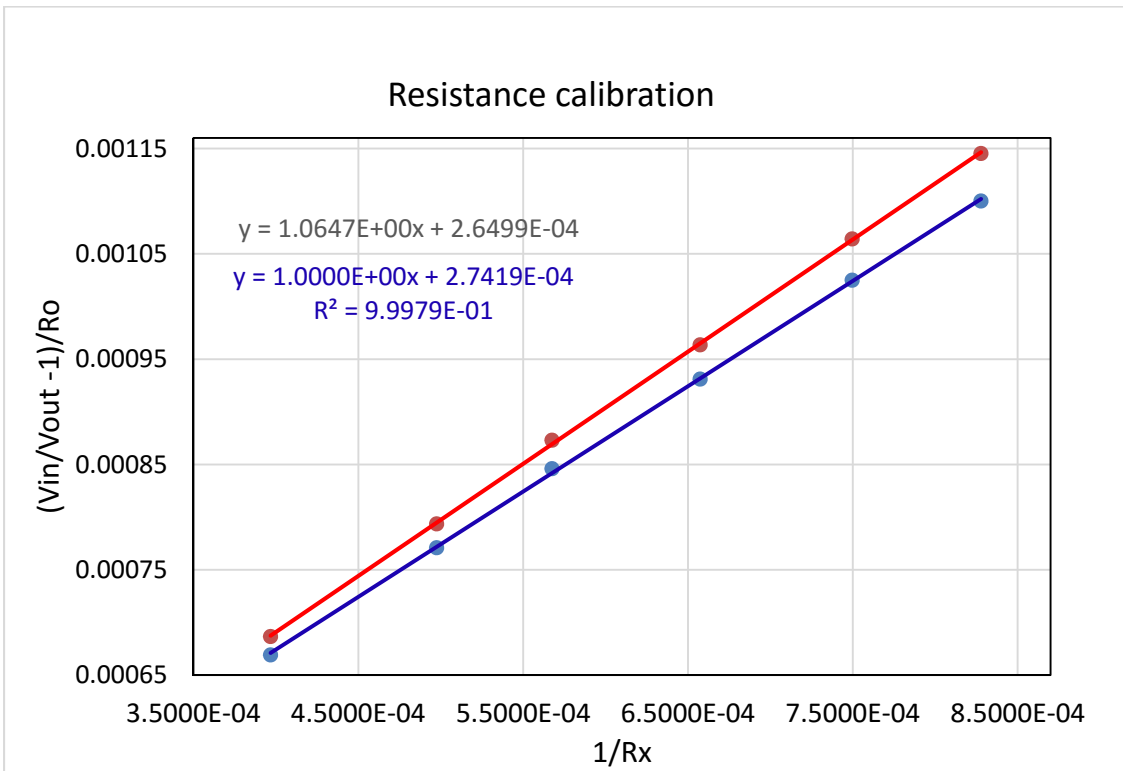measurements in this approach can be performed with accuracy better than 0.5%.

Figure S9. Plot of the signal variation in accordance to Equations S5 (red) and S6 (blue).

References

1. Masuda, H.; Fukuda, K. *"Ordered Metal Nanohole Arrays Made by a Two-Step Replication of Honeycomb Structures of Anodic Alumina,"* Science **1995**, 268, 1466–1468.

2. Masuda, H. *"Self-Ordering of Cell Arrangement of Anodic Porous Alumina Formed in Sulfuric Acid Solution,"* J. Electrochem. Soc. **1997**, *144*, L127.

3. Jessensky, O.; Muler, F.; Gösele, U. *"Self-Organized Formation of Hexagonal Pore Structures in Anodic Alumina,"* J. Electrochem. Society, **1998**, *72*, 1173–1175.

4. Li, A. P.; Müller, F.; Birner, A.; Nielsch, K.; Gösele, U. *"Polycrystalline Nanopore Arrays with Hexagonal Ordering on Aluminum,"* J. Vac. Sci. Technol. A Vacuum, Surfaces, Film. **1999**, *17*, 1428.

5. Ohgai, T.; Gravier, L.; Hoffer, X.; Lindeberg, M.; Hjort, K.; Spohr, R.; Ansermet, J-Ph.; *"Template Synthesis and Magnetoresistance Property of Ni and Co Single Nanowires Electrodeposited into Nanopores with a Wide Range of Aspect Ratios.",* J. Phys. D: Appl. Phys., **2003**, *36*, 3109–3114

6. Han, C. Y.; Willing, G. A.; Xiao, Z.; Wang, H. H. *"Control of the Anodic Aluminum Oxide Barrier Layer Opening Process by Wet Chemical Etching"* Langmuir **2007**, *23*, 1564–1568.

7. Santos, A.; Voikuvka, L.; Ferré-Borrull, J.; Marsal, L.F. *"In Situ Electrochemical Dissolution of the Oxide Barrier Layer of Porous Anodic Alumina Fabricated by Hard Anodization"* J. Electroanal. Chem. **2009**, *632*, 139–142

8. Garcia-Vergara, S. J. P.; Iglesias-Rubianes, L.; Blanco-Pinzon, C.E.; Skeldon, P.;

Thompson, G.E.; Campestrini, P. "*Mechanical Instability and Pore Generation in Anodic Alumina*" Proc. R. Soc. A **2006**, *462*, 2345–2358.

9. Brown, G.E.; Henrich, V.E.; Casey, W.H.; Clark D.L.; Eggleston, C.; Felmy, A.; Goodman, D.W.; Gratzel, M.; Maciel, G.; McCarthy, M.I.; Nealson, K.H.; Sverjensky, D.A.; Toney, M.F.; Zachara, J.M. "*Metal Oxide Surfaces and Their Interactions with Aqueous Solutions and Microbial Organisms.*" Chem. Rev. **1999**, *99*, 77–174

10. Penrod, S. L.; Olson, T. M.; Grant, S. B. *"Whole Particle Microelectrophoresis for Small Viruses,"* J. Colloid Interface Sci. **1995**, *173*, 521–523.

11. Schaldach, C. M.; Bourcier, W. L.; Shaw, H. F.; Viani, B. E.; Wilson, W. D. *"The Influence of Ionic Strength on the Interaction of Viruses with Charged Surfaces under Environmental Conditions,"* J. Colloid Interface Sci. **2006**, *294*, 1–10.

12. Langlet, J.; Gaboriaud, F.; Duval, J. F. L.; Gantzer, C. *"Aggregation and Surface Properties of F-specific RNA Phages: Implication for Membrane Filtration Processes,"* Water Res. **2008**, *42*, 2769–2777

13. http://www.daqarta.com/

14. http://www.ni.com/labview/